THE JOURNAL OF PHYSICAL CHEMISTRY B

Article

Molecular Simulation of the Influence of Interface Faceting on the Shock Sensitivity of a Model Plastic Bonded Explosive

Yunfeng Shi, and Donald W. Brenner

J. Phys. Chem. B, **2008**, 112 (47), 14898-14904 • Publication Date (Web): 31 October 2008

Molecular Simulation of the Influence of Interface Faceting on the Shock Sensitivity of a Model Plastic Bonded Explosive

Yunfeng Shi* and Donald W. Brenner

Department of Materials Science and Engineering, North Carolina State University, Raleigh, North Carolina 27587-7907

Received: June 28, 2008; Revised Manuscript Received: September 5, 2008

Molecular dynamics simulations are used to model the shock loading of an interface with various degrees of nanometer scale faceting between an inert binder and an energetic crystal. The facets create regions of local compression that induce exothermic reaction that leads to local hotspots and an increased shock sensitivity to detonation. Two mechanisms for compression and hotspot formation are identified that depend on the shock impedance mismatch between the binder and energetic crystal, namely shock focusing and local compression of the facets. These results provide a possible explanation for why spherical RDX crystals in cast polymer-bonded explosives appear less shock sensitive than RDX with more faceted morphologies.

I. Introduction

Despite decades of intensive research, understanding and ultimately controlling the shock sensitivity of high explosives remains one of the most challenging unsolved issues facing the energetic materials community. It is now well established that initiation originates from "hotspots" that can arise from the interaction of shocks with defects such as shear bands, heterogeneous interfaces, voids, and occlusions.[1] The details of this interaction, however, are not completely established and can differ widely from system to system. Chemical impurities, for example, can play a large role in hotspot formation and initiation, as can void collapse accompanied by adiabatic heating or jetting. The size of energetic crystals is also known to influence sensitivity, where small crystals are generally less sensitive than larger crystals.

The role of morphology and chemical purity in determining the sensitivity of so-called "reduced sensitivity" (RS) 1,3,5-trinitro-1,3,5-*s*-triazine (RDX) has been of continuing interest over the past two decades. van der Steen et al. initially reported that the shape of RDX crystals bound into a plastic bonded explosive (PBX) can have a large influence on sensitivity, with rounder crystals producing less sensitive materials.[2] Researchers at the French company Soci'et'e Nationale des Poudres et Explosifs subsequently reported the discovery of an RDX that when incorporated into a cast PBX significantly lowers the shock sensitivity.[3] The French researchers reported that their RS RDX, which is created by a recrystallization process, cannot be differentiated from conventional RDX by particle size, physical or chemical considerations, or the impact sensitivity of the neat crystals.[4] Follow-up studies by Australian researchers appear to confirm this result and also demonstrate that other RDX forms produced by other manufacturers can also lead to RS when cast into a PBX.[4] On the basis of examination of scanning electron micrographs, it appears that the crystals of all of the RS RDX tend to be more rounded than the other non-RS RDX forms.[4,5]

More recently, Doherty and Watt reported results from an extensive interlaboratory study of the chemical and physical properties (including impact and shock sensitivity) of seven types of RDX from five manufacturers.[6] These studies indicated that the impact sensitivity of neat samples of the various forms of RDX do not vary to a significant extent but that when cast into a PBX there are measurable differences in shock sensitivity between RS RDX and other forms of RDX. They also noted that the amount of HMX in each sample, which is a common impurity arising from the production of RDX, can have a profound influence on shock sensitivity. Most of the RS forms of RDX have a low HMX content, but this is not sufficient to guarantee RS. The role of crystal morphology was not explicitly addressed in this study.

Baer has used the CTH shock physics code to model the mesoscopic scale shock dynamics of packed neat HMX crystals and HMX crystals incorporated into a PBX.[7,8] He noted the formation of hotspots in the simulations from plastic flow and jetting into voids as well as from shock focusing due to differences in shock impedances in the material. For the packed crystal simulations, flow into the intercrystal regions was the dominant mechanism for hotspot formation. To probe the influence of crystal shape on shock properties, simulations of the shock loading of a regular array of spherical and cubic HMX crystals within a PBX were carried out, where the latter had a random rotational orientation. Larger pressure fluctuations were noted for the spherical crystals that arise from resonances in shock reflections due to the regular arrangement of crystals that are suppressed by the random rotations of the cubic crystals. A reactive model in which chemistry is initiated by a pressure threshold was also incorporated into a simulation of the shock compression of packed neat HMX crystals. A comparable study in a PBX, however, was not reported, and no further studies of the influence of crystal morphology or shock focusing on hotspot formation were noted.

Baer's modeling provides an explanation for why there is no difference in the impact sensitivity of neat crystals of RS and other RDX forms as reported by Doherty and Watt; hotspot formation and subsequent initiation is determined by material expansion in intercrystalline voids, which is largely unaffected by the purity or crystal morphology (for the same range of crystal sizes). However, it does not explain why the RS is manifest in the cast PBXs.

To further probe the possible role of crystal morphology on the sensitivity of cast PBXs, we have carried out molecular

* To whom correspondence should be addressed. E-mail: shiy2@rpi.edu.

10.1021/jp805690w CCC: $40.75
Published on Web 10/31/2008

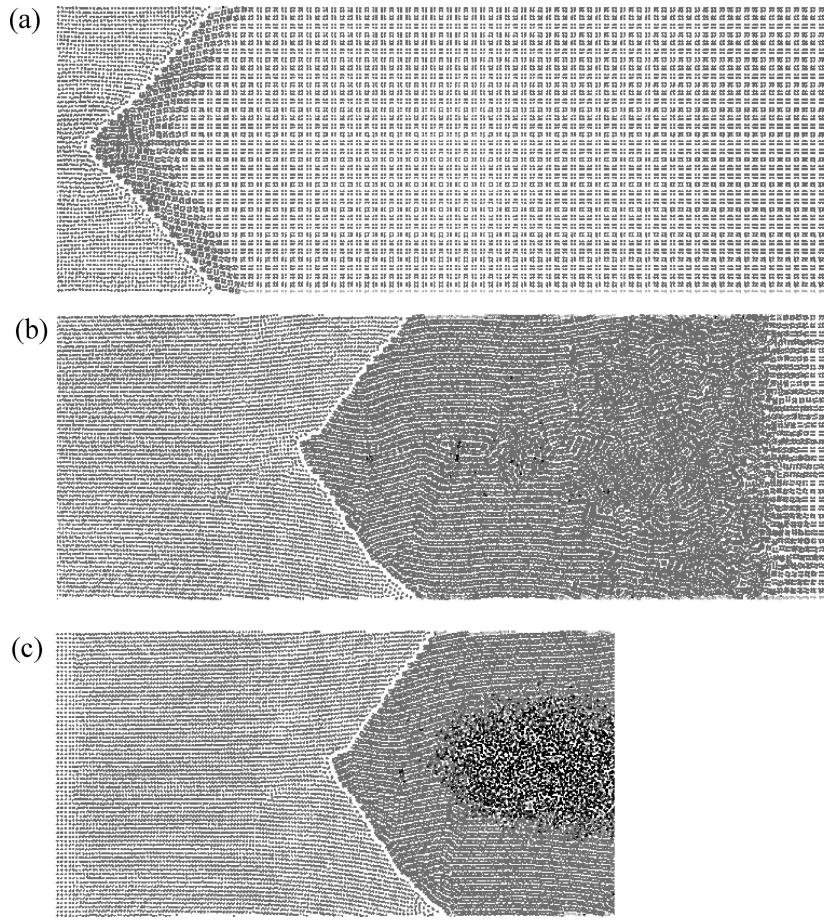

Figure 1. Illustrations of atomic configurations from a simulation of the shock loading of system I. The velocity of the driven piston is just above that needed for detonation. The atoms are colored according to their potential energy so that atoms with low potential energy appear darker. Time from frames (a)−(c) are 2.28, 8.36, and 14.44 ps, respectively.

dynamics simulations of the shock loading of interfaces with different degrees of nanometer-scale faceting between an inert binder and a model energetic crystal. Our simulations suggest that interface faceting can induce hotspots at specific locations, and for our model these hotspots can reduce the detonation threshold by as much as 24%. Two effects contribute to the mechanism of hotspot formation and enhanced sensitivity at a faceted interface depending on the shock impedance mismatch. When the velocity of a driven shock is larger in the binder than that in the energetic crystal, a planar shock front is refracted and focused toward the region between facets in the energetic crystal. This focusing is analogous to that reported by Baer in his mesoscopic scale modeling. In the second effect, the interface becomes flattened such that the tips of the facets that protrude into the binder are preferentially compressed. Unlike systems with a flat interface where detonation initiates randomly, the location of the hotspot for systems with a faceted interface is determined by the above mechanisms.

II. Computational Model

The simulated binder−crystal interface used in this study is composed of a model nitrogen cubane crystal and a single-component inert binder. For nitrogen, a recently developed reactive state summation (RSS) potential is used.[9] This potential is designed to model the exothermic dissociation of nitrogen cubane molecules into diatomic nitrogen molecules. This potential has been tested in thermal decomposition, mechanical shock, and void collapsing simulations in three-dimensional systems.[9,10] Steady detonation has been observed to propagate at an intrinsic speed. A pair-additive Morse potential was used for the binder−binder interactions.

$$E_{B-B}(r_{ij}) = \varepsilon_{B-B}(e^{2\rho_{B-B}(\sigma_{B-B}-r_{ij})} - 2e^{\rho_{B-B}(\sigma_{B-B}-r_{ij})}) + \varepsilon_{B-B}^{shift} \quad (1)$$

where ε_{B-B} is 0.0003 eV, ρ_{B-B} is 8.0 Å^{-1}, σ_{B-B} is 3.0498 Å, and $\varepsilon_{B-B}^{shift}$ is 2.21×10^{-6} eV. The cutoff is 3.75 Å. The interaction between nitrogen and binder atoms is modeled by a truncated and shifted Lennard-Jones potential

$$E_{B-N}(r_{ij}) = 4\varepsilon_{B-N}((\sigma_{B-N}/r_{ij})^{12} - (\sigma_{B-N}/r_{ij})^{6}) + \varepsilon_{B-N}^{shift} \quad (2)$$

where ε_{B-N} is 1.0 eV, σ_{B-N} is 3.3409 Å, and $\varepsilon_{B-N}^{shift}$ is 1.0 eV. The cutoff is 3.75 Å, which is the interatomic distance corresponding to the energy minimum. Therefore, this interaction is purely repulsive.

A thin slab geometry was used for the composite. The system contains about 40 000 binder atoms and 200 000 nitrogen atoms and has initial dimensions of $93.2 \times 35.5 \times 0.86$ nm^3. The system is periodic in the *Y* and *Z* directions, with the *X* direction being the shock direction. The nitrogen cubane molecules and the binder atoms are both in their energy minima and were initially packed with a lattice constant 0.4313 nm[9] in a simple cubic and a face-centered cubic lattice, respectively. This

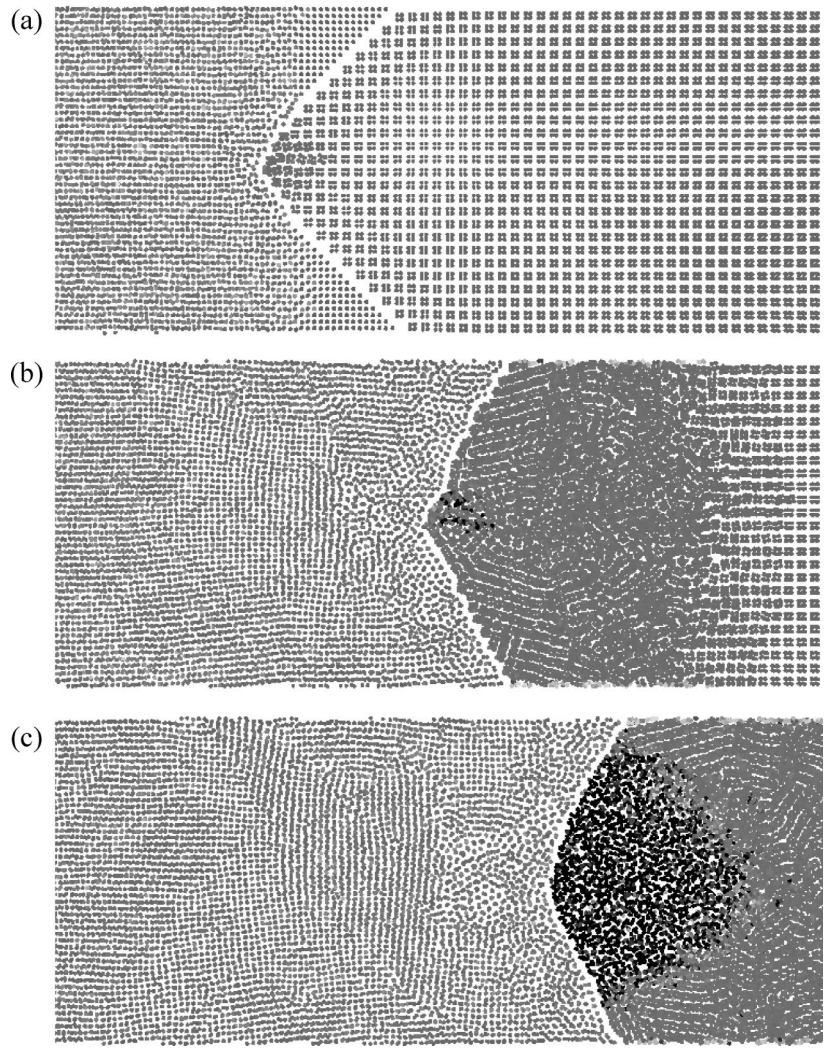

Figure 2. Illustrations of atomic configurations from a simulation of the shock loading of system III. The velocity of the driven piston is just above that needed for detonation. The atoms are colored according to their potential energy so that atoms with low potential energy appear darker. Time from frames (a)−(c) are 3.80, 6.84, and 9.12 ps, respectively.

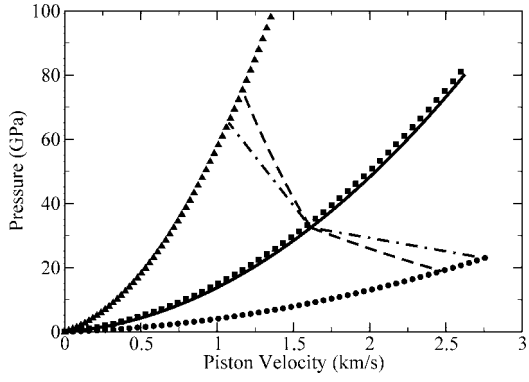

Figure 3. Shock Hugoniots for the binders in system I (circles), II (squares), and III (triangles) and the energetic crystal (solid line). The Hugoniots are parabola fits assuming shock velocity scales linearly with piston velocity. On the basis of the mirror-reflection Hugoniot approximation, the reshock (lower-right dashed line for system I) and decompressive isentrope lines (upper-left dashed line for system III) are drawn from the detonation threshold for the pure explosive. The dot-dashed straight lines have a slope of the negative of the initial binder density times the shock velocity according to the acoustic approximation. The detonation threshold is the intersection point of those lines with the binder's Hugoniot.

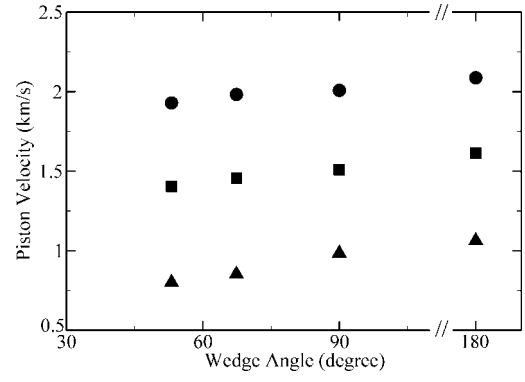

Figure 4. Threshold piston velocities as a function of interface angle for system I (circles), II (squares), and III (triangles). A flat interface has an angle of 180°. The measured threshold values have an accuracy of ±0.013 km/s.

produces a mechanically stable configuration and creates a coherent interface between the binder and energetic crystal. The ⟨100⟩, ⟨010⟩, and ⟨001⟩ directions of both the binder and the energetic crystal are parallel to the *X*, *Y*, and *Z* directions of the simulation box, respectively. Shock simulations on composite systems with binder's and explosive's <110> and <111> directions parallel to the *X* direction (the shock direction) as well as systems that are twice as large in the *Z* direction have shown the same results regarding the location of the hotspots and reduced detonation threshold due to interface geometries.

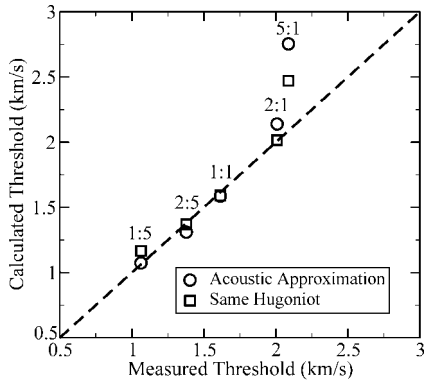

Figure 5. Threshold piston velocities calculated from eqs 3 and 4 plotted against threshold velocities determined from the simulations for five density ratio (ρ_X^0/ρ_B^0) as labeled in the plot.

Both the binder and energetic crystal were first cut to matching shapes and then brought to close contact to form either infinite flat interfaces (analogous to a PBX with spherical explosive particles) or zigzag interfaces (analogous to a PBX with faceted particles), as illustrated in Figures 1a and 2a. The average thickness of the binder is approximately the same for all interface shapes. The system starts at 0 K, and there is no temperature or pressure control in the subsequent MD simulations. A supported shock is created by displacing the first layer of the binder atoms at a constant rate toward the composite interface. The system is considered to detonate when the potential energy of the energetic crystal, which continuously increases due to shock compression, reaches a maximum and starts to decrease as a result of extensive exothermic reactions. Prior studies have shown that once this criterion is met, further dynamics with this potential will lead to a steady-state detonation. Minimum piston velocities needed to initiate detonation were determined by performing multiple simulations with different piston velocities which is similar to ref 10.

Three composite systems with different masses for the binder particles (and hence different densities) but identical atomic interactions were used to study how shock impedance matching affects the detonation threshold. The density ratio of binder over energetic crystal is 1/5, 1, and 5 for systems I, II, and III, respectively. The parameters for the binder−binder interaction were chosen so that the shock velocity of the binder in system II and the energetic crystal is identical within the range of piston speeds investigated here. Therefore, the shock velocity of the binder in system I (III) is always higher (lower) than that of the explosive given the same piston speed. Consequently, as shown in Figure 3, the pressure−piston velocity Hugoniot curves of the binders in system I, II, and III are below, on top of, and above that of the energetic crystal, respectively.

III. Results

Snapshots from simulations of systems I and III are illustrated in Figures 1 and 2, respectively, for a faceted interface with a facet angle of 90°. In both cases the piston velocity is above that needed to initiate detonation. As the rigid piston compresses the binder, an initially planar shock front is generated in the binder that propagates along the *X* direction. As the shock front propagates through the binder, extensive plastic damage is generated (cf. Figure 2c). For system I, where the shock impedance of the energetic crystal is larger than that of the binder, compressive reshock waves reflect back into the binder. In contrast, for system III, where the impedance of the energetic crystal is larger than that of the binder, decompression waves reflect back into the binder. For system II, where the shock impedance of the binder and crystal match, there are no reflection waves, and all of shock is transmitted from the binder to the crystal. Thus, the transmitted pressure inside the energetic crystal is greater, equal to, or smaller than the pressure of the compressed binder for system I, II, and III, respectively.

Detonation of the energetic crystal after the shock travels through the interface depends on the velocity of the driven piston. Plotted in Figure 4 is the minimum piston velocity needed to initiate detonation as a function of the wedge angle of the interface for the three systems. There are two important features to this data. First, the threshold piston velocity decreases with increasing density (mass) of the binder. Second, for each system the threshold piston velocity decreases monotonically with decreasing facet angle. To quantitatively understand the first feature, we focus on systems with flat interfaces. The full derivation of the two equations below will be given in the Appendix.

It can be assumed that the interface between the binder and the energetic crystal acts as a piston, and at the threshold detonation conditions the interface velocities and the pressure at the interface for different composites are identical and should be equal to that required to initiate detonation of the pure energetic system (measured in prior studies to be 1.61 km/s and 32.5 GPa). If the shock speed D of the binder and the explosive is linearly related to the piston speed U such that $D = a + bU$, the threshold piston velocity can be calculated under an acoustic approximation as[11,12]

$$U_B^{Th} = \frac{-2a_B + b_B U_X^{Th} + \sqrt{(2a_B + b_B U_X^{Th})^2 + 8b_B(a_X + b_X U_X^{Th})\rho_X^0/\rho_B^0 U_X^{Th}}}{4b_B} \quad (3)$$

where U_B^{Th} is the threshold piston velocity for a composite system and U_X^{Th} is that of the pure explosive, and ρ_X^0 and ρ_B^0 are the initial densities of the explosive and the binder, respectively. Alternatively, the piston velocity and pressure of the binder can be related to those of the interface by the reshock Hugoniot (in the case of system I) or the decompression isentrope (in the case of system III). Assuming those curves are mirror reflections of the principal Hugoniot of the binder (see ref 13), the detonation threshold in terms of binder piston velocity can be calculated as

$$U_B^{Th} = \frac{-a_B + 2b_B U_X^{Th} + \sqrt{a_B^2 + 4b_B(a_X + b_X U_X^{Th})\rho_X^0/\rho_B^0 U_X^{Th}}}{4b_B} \quad (4)$$

Given in Figure 5 are threshold piston velocities for systems with the flat interfaces calculated from eqs 3 and 4 plotted against the values determined from the simulations. Data are given for systems I, II, and III together with two additional binder/energetic crystal combinations with intermediate density ratios. Except for the composite with the lightest binder, both equations predict the threshold values within 10% of that determined from the simulations. This level of agreement is sufficient to establish that the difference in threshold piston

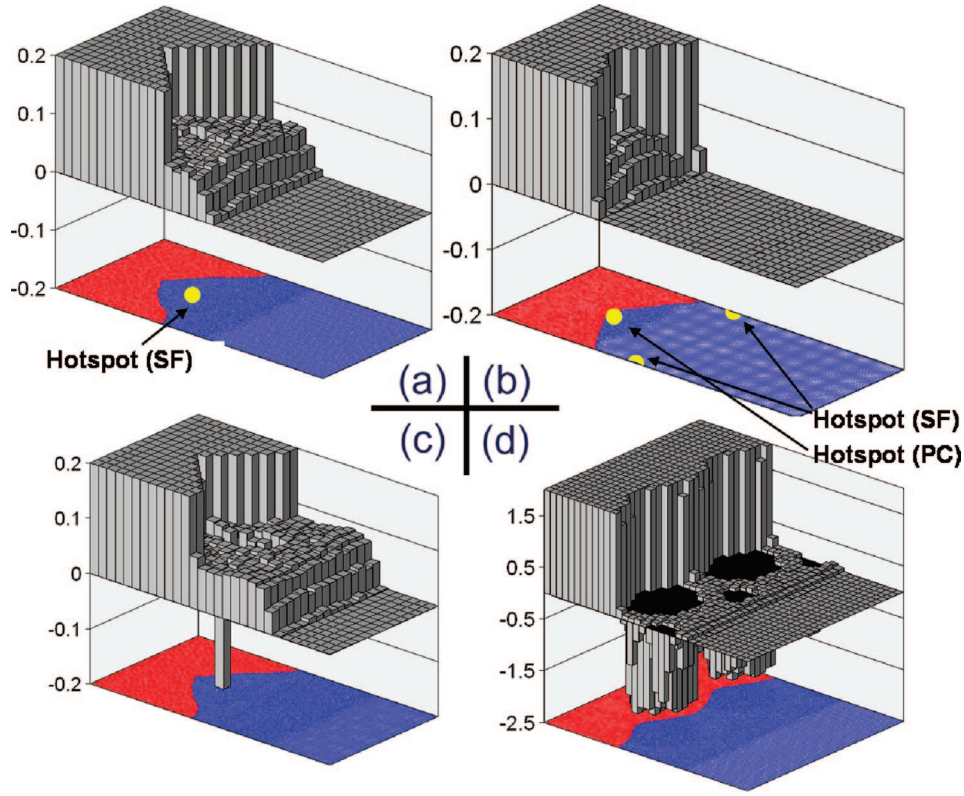

Figure 6. Coarse-grained potential energy (relative to the unperturbed explosive in units of eV/atom) and illustrated snapshots for an initial 90° facet for system I (panes a−c) and system III (panes b−d). Panes (a, b) are before and (c, d) are after the onset of detonation. The entire simulation cell is illustrated except for pane (d), where the system is doubled in the *Y* direction for better illustration of the hotspot. Yellow dots in panes (a, b) indicate the locations of the hotspots from shock focusing (SF) and preferential compression (PC). The piston speeds are just above the detonation threshold for each system (2.021 and 0.998 km/s for systems I and III, respectively). Binder atoms are red and nitrogen atoms are blue.

velocities for the flat interfaces is due mainly to shock impedance mismatch.

Detailed analysis of the simulation dynamics revealed two mechanisms that are responsible for the dependence of the threshold piston velocity on the facet angle. For system I, the effective piston speed for compression of the energetic crystal (the interface speed) is slower than the piston speed of the binder, and hence the shock front slows down as it propagates from the binder to the energetic crystal. This causes bending of the shock front and focusing of the shock pressure into the region of the energetic crystal between the facets. The degree of bending of the shock front away from the original shock direction, and hence the amount of focusing, increases for sharper interfaces. Illustrated along the bottom of the box in Figure 6a are the atomic coordinates for system I projected onto a single plane just after a shock front passes a faceted interface. The velocity of the piston driving the shock is just above the threshold velocity for detonation. The atoms in the binder and energetic crystal are red and blue, respectively, and the yellow dot indicates the position at which the hot spot will form. The three-dimensional bar graph above the atom positions indicates the corresponding coarse-grained potential energy of the atoms. There is a local increase in the potential energy due to shock focusing at the point where the hotspot will form. Figure 6c illustrates the same system a little further in the trajectory. The shock front, which is visible as the sudden increase in the potential energy bar graph, has moved further into the energetic crystal. The increase in potential energy between the facets in the energetic crystal due to focusing was sufficient to overcome the barrier for reaction, and the potential energy has dropped at this local point as exothermic reaction is initiated. This drop in potential energy results in a corresponding increase in local kinetic energy—the hotspot—that grows and transitions into the detonation.

Panels b and d in Figure 6 illustrate the same quantities for system III as those considered for panels a and c for system I. The yellow dots in panel b indicate two places where hotspots will form (one of the dots skirts the periodic boundaries). The dots labeled SF arise from shock focusing as in system I. However, because the effective piston speed for compression of the energetic crystal (the interface speed) is *faster* than the piston speed of the binder, the focusing occurs at points in the energetic crystal near where the tips of the binder protrude into the energetic crystal. As in system I, this focusing locally raises the potential energy. The second hotspot for this system occurs between the facets as in system I but is located closer to the interface than in system I. This second hot spot is due to a flattening of the interface and hence preferential compression of the facets. It is apparent from the localized drop in the potential energy visible in the bar graph in panel d in Figure 6 that both the shock focusing and facet compression are sufficient to induce exothermic reactions. For this system, however, the hotspot and subsequent initiation of detonation occur more readily from the latter.

IV. Summary

The simulations reported herein were motivated by the recent interest in understanding the origin of the RS reported for several grades of RDX and specifically to explore how a smoother crystal embedded within an inert matrix might reduce the sensitivity of a PBX. Our simulations demonstrate that a nanometer-scale faceted interface structure between a binder and

energetic crystal can influence sensitivity via two mechanisms: shock focusing and facet compression. How these two mechanisms translate to larger scales is unclear; however, based on the shock focusing noted by Baer the former mechanism likely operates at the grain scale.

Acknowledgment. We thank D. Thompson, T. Sewell, Y. Hu, and B. Broom for stimulating discussions. Molecular dynamics simulations were carried out in LAMMPS.[14,15] Computational resources are provided by HPC-NCSU. This work was supported by a MURI project from the U.S. Army Research Office.

Appendix. Derivations of Detonation Thresholds for PBXs with Flat Interfaces.

The detonation thresholds for energetic composites with flat interfaces are given in eqs 3 and 4 in the main text. In a PBX system, the detonation threshold, as characterized by the piston velocity that drives the binder, is different than that for the pure explosive. This is due to impedance mismatch between the binder and the explosive. From the continuity conditions across the binder and explosive interface, one can calculate the detonation threshold values for the PBXs based on the threshold values for the pure explosive as well as the material properties of the binder. The derivation will be given here.

We assume a linear relationship between the piston speed U and the shock speed D, so that

$$D_B = a_B + b_B U_B \tag{A1}$$

$$D_X = a_X + b_X U_X \tag{A2}$$

Here a and b are materials constants that can be obtained via a linear fitting from our simulation data. Subscript B denotes the binder and X denotes the explosive. From mass conservation and momentum balance

$$P_B = \rho_B^0 U_B D_B \tag{A3}$$

$$P_X = \rho_X^0 U_X D_X \tag{A4}$$

Here P_B and P_X are pressures of the compressed state inside the binder and explosive being driven by a piston. Note that eqs A3 and A4 describe the behavior of isolated binder and explosive. In a PBX composite, since the binder is driven directly by the piston, eq A3 remains valid. ρ_B^0 and ρ_X^0 are initial densities for the binder and the explosive.

Based on the assumption that, at threshold detonation, the interface pressure/velocity equals the threshold detonation pressure/piston speed for a pure explosive, the PBX interface is essentially a piston driving the explosive. Thus

$$P_I = P_X^{Th} = \rho_X^0 U_X^{Th} D_X^{Th} = \rho_X^0 U_X^{Th}(a_X + b_X U_X^{Th}) \tag{A5}$$

$$U_I = U_X^{Th} \tag{A6}$$

Here P_I and U_I are the interface pressure and velocity in a PBX setting. U_X^{Th} is the threshold piston speed for a pure explosive to detonate.

Now we need one additional relation from one of the following approximations that originate from continuity across the binder−explosive interface. Please note that these two approximations give very close results that agree with the molecular dynamics simulation results reasonably well, as shown in Figure 5.

Acoustic Approximation. Based on the acoustic approximation (refs 11 and 12)

$$\frac{P_B - P_I}{U_B - U_I} = -\rho_B^0 D_B \tag{A7}$$

Substituting P_B, P_I, D_B, and U_I using eqs A3, A5, A1, and A6, eq A7 becomes

$$\frac{\rho_B^0 U_B(a_B + b_B U_B) - \rho_X^0 U_X^{Th}(a_X + b_X U_X^{Th})}{U_B - U_X^{Th}} = -\rho_B^0(a_B + b_B U_B) \tag{A8}$$

Solving the above quadratic equation for U_B and two solutions can be obtained. It can be shown that these two solutions have opposite signs therefore the negative solution is discarded. Thus, the threshold piston speed for the energetic composite is (same as eq 3 in the main text)

$$U_B^{Th} = \frac{-2a_B + b_B U_X^{Th} + \sqrt{(2a_B + b_B U_X^{Th})^2 + 8b_B(a_X + b_X U_X^{Th})\rho_X^0/\rho_B^0 U_X^{Th}}}{4b_B} \tag{A9}$$

Mirror-Reflection Hugoniot Approximation. Based on the mirror-reflection Hugoniot approximation (ref 13), the reshock or the decompressive isentrope for the binder is the mirror reflection (around $U = U_B$) of the primary Hugoniot of the binder (eq A3). Therefore, it has the following functional form in the pressure vs piston speed domain:

$$P = \rho_B^0(2U_B - U)(a_B + b_B(2U_B - U)) \tag{A10}$$

This reshock/decompressive curve intersects with the Hugoniot of the explosive at (U_I,P_I). Therefore, (U_I,P_I) satisfies eq A10

$$P_I = \rho_B^0(2U_B - U_I)(a_B + b_B(2U_B - U_I)) \tag{A11}$$

Again substituting P_I and U_I using eqs A5 and A6

$$\rho_X^0 U_X^{Th}(a_X + b_X U_X^{Th}) = \rho_B^0(2U_B - U_X^{Th})(a_B + b_B(2U_B - U_X^{Th})) \tag{A12}$$

Solving the above equation for U_B and two solutions can be obtained. One of them is negative for the parameters from molecular dynamics simulations. Thus, the threshold piston speed for the energetic composite is (the same as eq 4 in the main text)

$$U_B^{Th} = \frac{-a_B + 2b_B U_X^{Th} + \sqrt{a_B{}^2 + 4b_B(a_X + b_X U_X^{Th})\rho_X^0/\rho_B^0 U_X^{Th}}}{4b_B} \quad \text{(A13)}$$

References and Notes

(1) Field, J. E. *Acc. Chem. Res.* **1992**, *25*, 489.

(2) van der Steen, A. C.; Verbeek, H. J.; Meulenbrugge, J. J. *9th Symposium (International) on Detonation*; OCNR: Arlington, VA, 1989; p 83.

(3) Lecume, S.; Chabin, P.; Brunet, P. 2001 Insensitive Munitions and Energetic Materials Symposium, Bordeaux, 2002.

(4) Lochert, I. J.; Franson, M. D.; Hamshere, B. L. Defence Science and Technology Report DSTO-TR-1447, DSTO Science Systems Laboratory, **2003**.

(5) van der Heijden, A. E. D. M.; Bouma, R. H. B. *Cryst. Growth Des.* **2004**, *4*, 999.

(6) Doherty, R. M.; Watt, D. S. *Propellants, Explos., Pyrotech.* **2008**, *33*, 4.

(7) Baer, M. R. *Thermochim. Acta* **2002**, *384*, 351.

(8) Baer, M.; Sewell, T. *Molecular Dynamics Simulations of Detonation Phenomena*; ITRI Press: Laurel, MD, 2004; Chapter 5.

(9) Shi, Y. F.; Brenner, D. W. *J. Chem. Phys.* **2007**, *127*, 134503.

(10) Shi, Y. F.; Brenner, D. W. *J. Phys. Chem. C* **2008**, *112*, 6263.

(11) Duff, R. E.; Houston, E. *J. Chem. Phys.* **1955**, *23*, 1268.

(12) Deal, W. E. *J. Chem. Phys.* **1957**, *27*, 796.

(13) Davison, L.; Graham, R. A. *Phys. Rep.* **1979**, *55*, 255.

(14) Plimpton, S. J. L.A.M.M.P.S. Molecular Dynamics Simulator (http://lammps.sandia.gov).

(15) Plimpton, S. J. *J. Comput. Phys.* **1995**, *117*, 1–19.

JP805690W